THREE-DIMENSIONAL FINITE-ELEMENT MODELS OF CYLINDRICAL WOOD FIBERS

J. D. Barrett
Department of the Environment, Canadian Forestry Service
Western Forest Products Laboratory, Vancouver, British Columbia

and

A. P. Schniewind
University of California, Forest Products Laboratory, Richmond, California

(Received 5 July 1973)

ABSTRACT

A finite-element solution is presented for analysis of concentric, multilayered, orthotropic cylinders subjected to loadings that do not vary around the circumference. Model fibers are analyzed, and stress distributions are compared to those obtained, using a closed form solution technique. The influence of boundary-shear restraint on internal stress distribution is studied. Comparing results of the three-dimensional finite-element model to values of axial stiffness and relative twisting angles predicted using simpler, two-dimensional methods indicated that the two-dimensional models can give good estimates of these parameters, at least for the thin-walled models.

Additional keywords: Mathematical analysis, layered systems, finite element, cell mechanics.

Symbols

A	Cell-wall cross-section area
B	Strain matrix
C_{ij}	Elastic compliances
D	Matrix of elastic compliances
E_{rr},E_{tt},E_{zz}	Moduli of elasticity
G_{rt},G_{rz},G_{tz}	Shear moduli of elasticity
P	External axial force
P_j	Layer volume proportion
p	Internal or external pressure
r,t,z	Coordinate directions
$\hat{S}_{ij}$	Composite-layer compliance component
u,v,w	Displacement components
u_i,v_i	Nodal displacements
$v_{2.0}$	Displacement at z = 2.0 cm
α	An angle
γ_{rt},γ_{rz},γ_{tz}	Shear strain components
δ	Vector of element displacement components
ϵ_{rr},ϵ_{tt},ϵ_{zz}	Normal strain components
ϵ_0	Specified strain component
η,ξ	Local element coordinates
θ	Coordinate direction
μ_{ij}	Poisson's ratios
σ_{rr},σ_{tt},σ_{zz}	Normal stress components
σ_{rt},σ_{rz},σ_{tz}	Shear stress components
$\hat{\sigma}$	Axial stress
ϕ	Twist angle

Superscripts

'(prime)	Coordinate system parallel and perpendicular to microfibrils
e	Element property
T	Transpose of vector or matrix quantity

Subscript

j	j^{th} layer property

INTRODUCTION

In approaching the three-dimensional elastic analysis of wood fibers, the simplest logical geometric model appears to be the circular cylinder. Solutions for the distribution of stresses and displacements in circular isotropic and orthotropic cylinders have been available for many years for some specific loading conditions (Timoshenko and Goodier 1951; Lekhnitskii 1963). A general treatment of the state of stresses in a multilayered system of concentric, anisotropic cylinders subjected to axial

loading does not appear to be available in closed form.[1] Tang (1972) attempted to solve for stress distributions in a four-layered anisotropic cylinder subjected to an axial force using the single orthotropic cylinder analysis of Lekhnitskii (1963). The single layer analysis that was used to model the individual-layer behavior predicts that the cylinder will twist in general, because of the application of axial forces. Twisting results from the fact that the axes of material symmetry are in general oriented at an angle to the cell axis direction. The amount of twisting depends on the material properties and the orientation angle. In the multilayered cell subjected to axial loading, layers twist as a unit and, therefore, internal stresses develop because of the restraint of potential deformation of the individual layers. Interlayer compatibility was achieved by matching boundary conditions, in terms of stresses and displacements at layer interfaces, thereby providing an estimate of multi-layered-cylinder response.

Unfortunately, one of the boundary conditions chosen by Tang does not appear to be rational. He specified that at the boundary between layers, on the tangential-longitudinal plane the σ_{tz} shear stress at the outer edge of the inner layer must be equal to the σ_{tz} shear stress at the inner edge of the outer layer. While this requirement may appear reasonable, it is not valid because it implies that layers are free to twist with respect to each other, which in a normal wood fiber clearly is not the case. It would have been more rational to specify equal transverse displacements at the interface, although within the solution scheme given by Lekhnitskii (1963) this is not readily accomplished. Using this assumption, in addition to specifying equal radial displacements and radial stresses at the contacting interlayer surfaces, would have provided a more rational set of boundary conditions.

As a result of the particular boundary conditions adopted by Tang, rather large and diverse twisting angles are calculated for the various cell-wall layers, despite the fact that in a real fiber the various layers will have to twist as a unit. Furthermore, Tang then assumed that the angle of twist is equal in all layers in order to calculate the total twisting of a fiber. This, in turn, would imply the introduction of additional shear stresses which, however, are not considered in the stress analysis given by Tang. Consequently his analysis scheme has some serious flaws in concept.

The flaws become further evident if one examines the numerical results obtained by Tang. One would expect that integration of the normalized axial layer stresses over the total cell-wall area would yield unity, since the stresses are normalized with respect to the external stress. Using maximum and minimum values for each layer from Table 6 of Tang (1972) to calculate bounds on the integral, its value is found to be between –1.52 and –1.54 for tangential walls and between –1.18 and –1.26 for radial walls, both in Case 3. Not only do the integrals differ appreciably from unity, but also they are negative, indicating axial layer stresses opposite in sign from the applied external stresses. Similarly, tangential stresses should integrate to zero over the radius to maintain equilibrium, but for Case 3 integral relative stresses of –1.06 and –0.18 are obtained for tangential and radial walls, respectively.

In view of these difficulties, it is not surprising that substantial differences were observed by Tang between the results of his three-dimensional analysis and those of the two-dimensional analysis of Mark and Gillis (1970). The specific comparison is not valid in any case for two reasons. First, Mark and Gillis used complete shear restraint without stating this explicitly (i.e. the in-plane shear strain specified as zero) and, second, they gave stresses parellel and perpendicular to the microfibril in each layer, while Tang's data refer to the co-

[1] Very recently, Gillis and Mark (1973) presented a closed-form solution for stresses in laminated, concentric, orthotropic cylinders. The method is conceptually capable of predicting stresses under general loading conditions, but the method was used to study only effects of moisture-content changes.

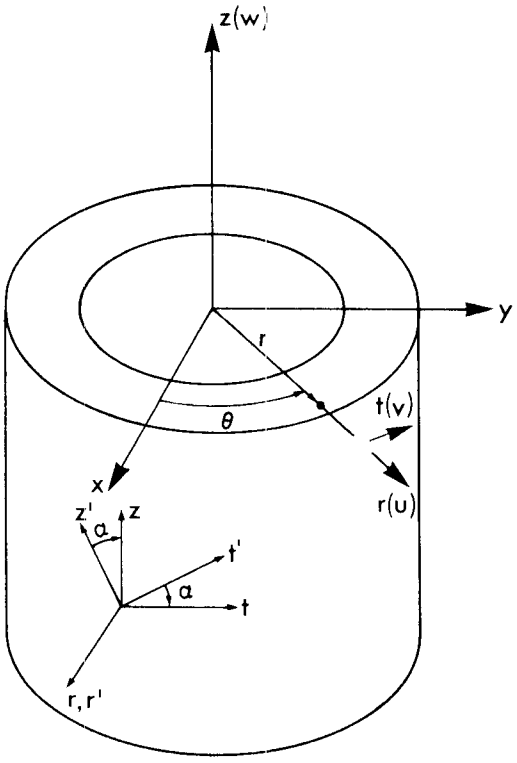

FIG. 1. Circular cylinder subjected to a boundary stress distribution independent of the θ coordinate. Axes of elastic symmetry for the orthotropic cell-wall material are inclined at angle α to axial direction.

ordinate system parallel and perpendicular to the longitudinal cell axis. The presence or absence of shear restraint (fiber aggregates vs. single fibers) is an important factor in determining the stress distribution obtained in a given model. Thus, it is not correct that the absence of shear stresses in the combined Middle lamella + Primary wall (M + P) is a feature of two-dimensional analysis, as suggested by Tang, but depends rather on the presence of shear restraint. Without complete shear restraint, shear stresses are found in M + P in the two-dimensional analysis (Schniewind 1972). It is also not correct that two-dimensional approaches cannot yield an estimate of fiber twisting because such an analysis has been made previously assuming a fiber to be a thin-walled cylinder (Schniewind and Barrett 1969).

The purpose of this study is to calculate the stress distribution in multilayered, concentric, anisotropic cylinders. Of particular interest is the radial distribution of stress induced by the application of an axial force. A general formulation allowing investigation of cylinder models subjected to axial forces, internal and external pressures with free and restrained boundaries is achieved conveniently using finite-element techniques presented. Axial forces will be introduced by specifying axial displacements in individual elements.

FINITE-ELEMENT MODELS

The circular cylinder of Fig. 1 is assumed to be subjected to distribution of stresses that are independent of the θ coordinate and possesses orthotropic material properties with respect to the z'r't' coordinate system. The axes of elastic symmetry are oriented at an angle α to the global (zrt) coordinate system. The constitutive law for the wall material, written with respect to the global coordinate system, is:

$$\{\sigma\} = [D]\,\{\varepsilon\} \tag{1}$$

where: $\{\sigma\}^T = \{\sigma_{rr}, \sigma_{tt}, \sigma_{tz}, \sigma_{zr}, \sigma_{rt}, \sigma_{zz}\}$

$$\{\varepsilon\}^T = \{\varepsilon_{rr}, \varepsilon_{tt}, \gamma_{tz}, \gamma_{zr}, \gamma_{rt}, \varepsilon_{zz}\}$$

$$\text{and } [D] = \begin{bmatrix} C_{11} & C_{12} & C_{14} & 0 & 0 & C_{13} \\ C_{21} & C_{22} & C_{24} & 0 & 0 & C_{23} \\ C_{41} & C_{42} & C_{44} & 0 & 0 & C_{43} \\ 0 & 0 & 0 & C_{55} & C_{56} & 0 \\ 0 & 0 & 0 & C_{65} & C_{66} & 0 \\ C_{31} & C_{32} & C_{34} & 0 & 0 & C_{33} \end{bmatrix} \tag{2}$$

if 1=rr, 2=tt, 3=zz, 4=zt, 5=zr, 6=tr;

C_{ij} are transformed elastic stiffnesses.

Since applied loads are assumed axially symmetric, the radial (u) and tangential (v) displacements are independent of the θ coordinate. Allowing for an axial variation of transverse displacement, we assume:

$$u = u(r,z)$$
$$v = v(r,z) \tag{3}$$

Planes perpendicular to the z axis are assumed to remain plane during deformation and the w displacement is assumed to have the following form:

$$w = w(z) = \varepsilon_o z \tag{4}$$

Using displacement assumptions of equations 3 and 4, the corresponding strains are computed in cylindrical coordinates neglecting terms where dependence of a strain component on the t coordinate is introduced, since no t dependence in strain, stress, or loading is allowed.

In cylindrical coordinates corresponding strains are given by[2]:

$$\begin{Bmatrix} \varepsilon_{rr} \\ \varepsilon_{tt} \\ \gamma_{tz} \\ \gamma_{zr} \\ \gamma_{rt} \\ \varepsilon_{zz} \end{Bmatrix} = \begin{Bmatrix} u_{,r} \\ u/r \\ v_{,z} \\ u_{,z} \\ v_{,r}-v/r \\ w_{,z} \end{Bmatrix} \tag{5}$$

Finite-element modelling can now be accomplished by dividing a longitudinal section passing through the axis of the cylinder into small elements. Each of the small elements in the section generates a ring-shaped solid of revolution (Fig. 2). Material properties can be specified separately for each element, which allows for modelling of the layered structure. Because of the special symmetry involved, the analysis is similar to those for plane stress and strain. Details are given by Zienkiewicz (1971) and only a brief summary will be presented here.

A quadrilateral, linear, isoparametric element of the "serendipity" type (Zienkiewicz 1971) is used to model radial and tangential displacements. Each element has the same axial strain $\epsilon_{zz} = \epsilon_0$. Displacement parameters associated with the element (Fig. 2) are therefore:

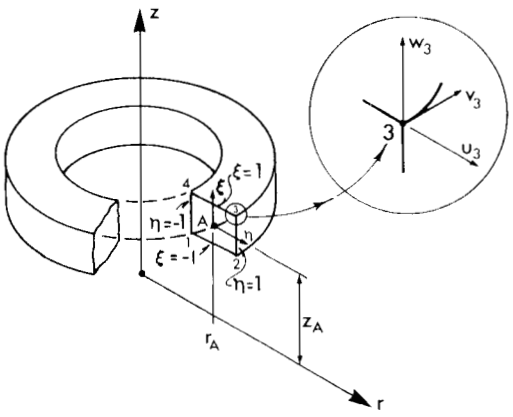

FIG. 2. Cylindrical ring element used for finite-element analysis showing normalized local coordinates and displacement modes of element.

$$\left|\{\delta\}^e\right|^T = \{u_1,v_1,u_2,v_2,u_3,v_3,u_4,v_4,\varepsilon_o\} \ . \tag{6}$$

Strains are given in terms of the displacement parameters according to:

$$\{\varepsilon\} = [B]\ \{\delta\}^e \ . \tag{7}$$

The displacement fields are expressed in terms of the shape functions N_1, N_2, N_3, and N_4 such that

$$u = \sum_{i=1}^{4} N_i u_i$$
$$v = \sum_{i=1}^{4} N_i v_i \tag{8}$$

where:

$$N_1 = (1-\xi)(1-\eta)/4$$
$$N_2 = (1-\eta)(1+\xi)/4$$
$$N_3 = (1+\eta)(1+\xi)/4$$
$$N_4 = (1+\eta)(1-\xi)/4$$

are the shape functions for the linear quadrilateral element in local coordinates. The strain matrix B is evaluated in terms of the local coordinates ξ,η of the normalized rectangle of Fig. 2. This matrix is presented in Fig. 3.

[2] $u_{,r}$ signifies $\delta u/\delta r$, etc.

$$[B] = \begin{bmatrix} N_{1,r} & 0 & N_{2,r} & 0 & N_{3,r} & 0 & N_{4,r} & 0 & 0 \\ \frac{N_1}{r} & 0 & \frac{N_2}{r} & 0 & \frac{N_3}{r} & 0 & \frac{N_4}{r} & 0 & 0 \\ 0 & N_{1,z} & 0 & N_{2,z} & 0 & N_{3,z} & 0 & N_{4,z} & 0 \\ N_{1,z} & 0 & N_{2,z} & 0 & N_{3,z} & 0 & N_{4,z} & 0 & 0 \\ 0 & N_{1,r}-\frac{N_1}{r} & 0 & N_{2,r}-\frac{N_2}{r} & 0 & N_{3,r}-\frac{N_3}{r} & 0 & N_{4,r}-\frac{N_4}{r} & 0 \\ 0 & 0 & 0 & 0 & 0 & 0 & 0 & 0 & 1 \end{bmatrix} \quad (9)$$

FIG. 3. Strain matrix B for axisymmetric quadrilateral finite element of Fig. 2.

The element stiffness matrix is given in global coordinates by:

$$[k]^e = \int_{vol} [B]^T [D] [B] \, dVol \quad (10)$$

where: $dVol = rdrd\theta$

To facilitate integration, the numerical integration was performed with respect to local coordinates η,ξ of Fig. 2 and was accomplished using a four-point Gaussian quadrature formula (Zienkiewicz 1971).

NUMERICAL STUDIES

Constrained thick-walled orthotropic cylinder

The finite-element analysis was evaluated by comparing finite element results with a closed form solution for the distribution of stresses in an axially constrained ($w = 0$ at $z = z_{max}$ or equivalently $\epsilon_{zz} = 0$), clamped ($v = 0$ at $z = z_{max}$) orthotropic cylinder subjected to an internal and external pressure (Lekhnitskii 1963). This closed form solution was chosen because deformation patterns and stress distributions resemble those expected in the cell models.

A suitable set of material parameters and internal and external pressures were chosen for purpose of comparison.

$E'_{rr} = 100$ $G'_{rz} = 50$ $\mu'_{rz} = 0.2$
$E'_{tt} = 300$ $G'_{rt} = 40$ $\mu'_{rt} = 0.3$
$E'_{zz} = 200$ $G'_{zt} = 30$ $\mu'_{zt} = 0.45$
$\alpha = 10°$

$p_{internal} = 9000$
$p_{external} = 15000$
(units of E′, G′ and p are dynes cm^{-2}).

Results of the analysis presented in Fig. 4 were derived using the discretization

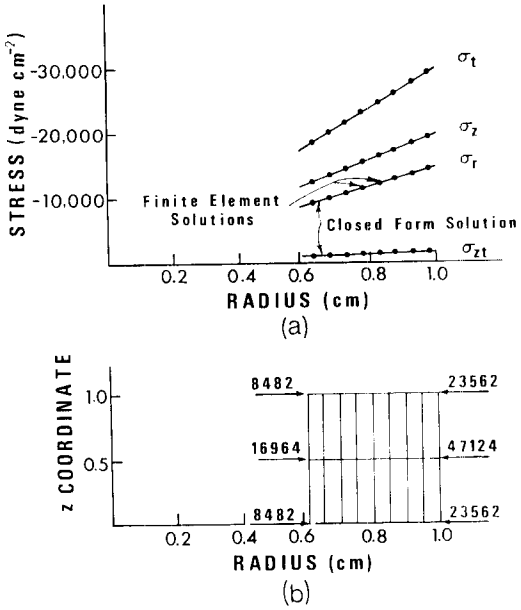

FIG. 4. a. Shear and normal stresses produced in a pressurized orthotropic cylinder with axial strains restrained and ends clamped; computed axial forces were –32629 dynes and –32791 dynes for the closed form and finite element methods respectively. b. Discretization scheme employed for finite-element analysis. Indicated specified forces correspond to applied internal and external pressures of 9,000 and 15,000 dyne cm^{-2} respectively.

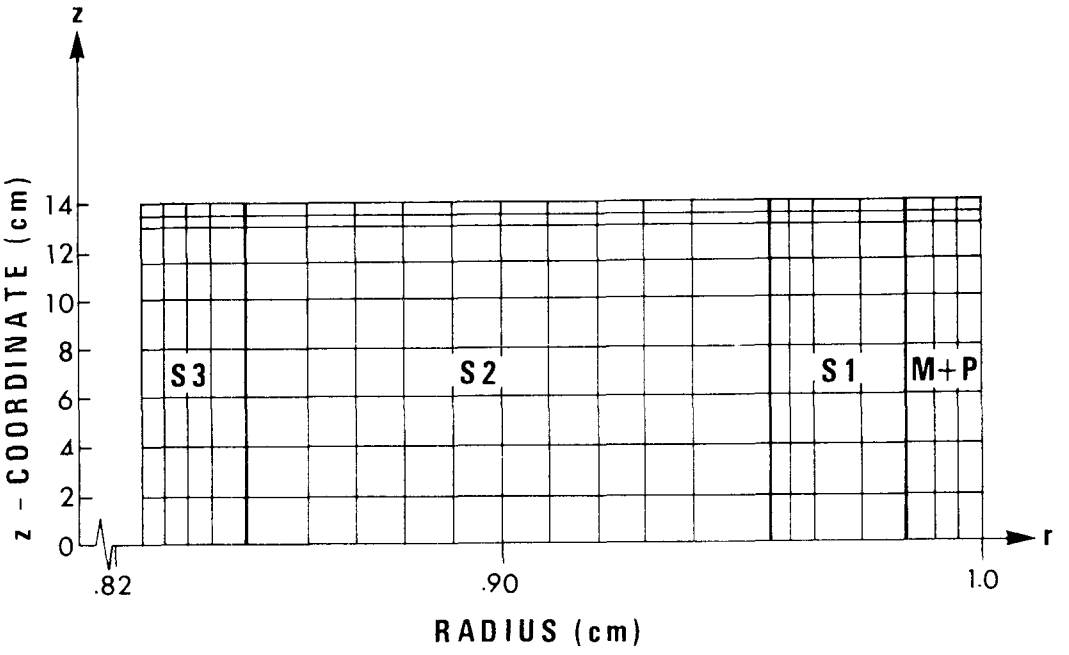

FIG. 5. Discretization scheme used for fiber model analyses.

scheme of Fig. 4. It may be seen that the plotted points from the finite-element results are in excellent agreement with the solid lines derived from the closed-form solution.

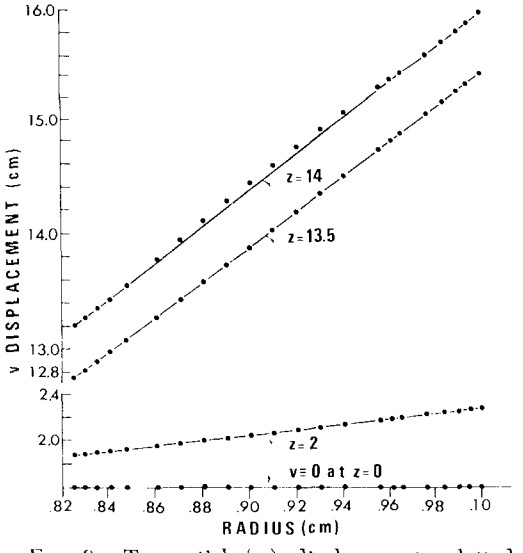

FIG. 6. Tangential (v) displacements plotted for value of z = 0, 2, 13.5, and 14 cm for model I-3.

Wood fiber models

The concentric orthotropic cylinder model has been employed by Tang (1972) to model the deformation of a wood fiber subjected to an axial force. Improvements in the analysis of these models can be achieved using the finite-element model previously described. Since the finite-element analysis is a displacement formulation, interlayer compatibility is automatically insured. Application of the finite-element analysis technique to wood fiber model analyses requires only that a discretization scheme be employed that recognizes the material inhomogeneity across a fiber wall.

The same six unrestrained models analyzed by Tang (1972)[3] were modelled using the discretization scheme of Fig. 5 so that effects of the analysis scheme on

[3] Models were either type I, representing radial cell walls with larger fibril angles in S_2 and S_3, or type II representing tangential walls. Each type was analyzed for three different sets of elastic constants for cellulose. The models are denoted I-1, I-2, I-3, II-1, II-2 and II-3.

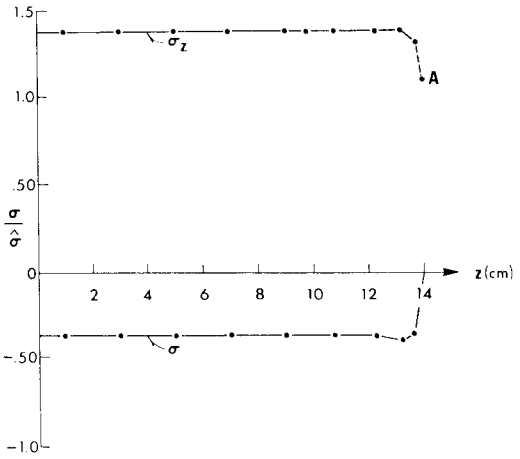

FIG. 7. Axial variation of σ_{zz} and σ_{tz} for model I-3 plotted for $r = 0.905$ cm. Shear stress σ_{tz} must be zero on the end surface since no shear stress or v displacement is specified. Normal stress σ_{zz} will generally be non-zero on end surface since w displacements are specified everywhere. Exact value of σ_{zz} at $z = 14$ is, however, not determined although $\int_A \sigma_{zz}/\hat{\sigma}\, dA = 1$ on the end surface.

computed results can be evaluated in comparison to the results presented by Tang (1972). Detailed results are presented only for model I-3. Figure 6 shows v displacements for model I-3 as a function of radius for constant values of z. From symmetry it can be shown that radial lines in these models should remain straight during deformation, and except for the end effects, this conclusion is verified by the finite-element results. The end effect results from the fact that σ_{zt} shear stresses may exist. Since σ_{zt} shear stresses are not specified along the upper boundary, the net twisting moment on any plane perpendicular to the z axis of the cylinder must be identically zero, but locally σ_{zt} shear stress goes to zero everywhere along the boundary $z = 14$. The v displacements along the line $z = 14$ are therefore not linear with respect to the radial coordinate. The variaiton of σ_{tz} and σ_{zz} with respect to z for model I-3 is plotted in Fig. 7 for $r = 0.905$ cm. Displacements and stresses predicted for the models studied are produced by a specified axial strain $\epsilon_z = \epsilon_0$ and $\epsilon_0 = 1$. The axial force P produced by this strain is given by

$$P = 2\pi \int_{r_{min}}^{r_{max}} \sigma_{zz} r\, dr \,. \tag{11}$$

A global axial stress is defined

$$\hat{\sigma} = \frac{P}{\pi(r_{max}^2 - r_{min}^2)} \tag{12}$$

and accordingly,

$$\frac{1}{A} \int_A \frac{\sigma_{zz}}{\hat{\sigma}}\, dA = 1 \tag{13}$$

but, for the Tang models, the cross-section area of cell-wall material is unity, therefore:

$$\int_A \frac{\sigma_{zz}}{\hat{\sigma}}\, dA = 1 \,. \tag{14}$$

The v displacement of the outer boundary of the unrestrained fiber model I-3 is shown in Fig. 8 as a function of z with a straight line fitted through zero and the lower linear portion of the plotted data. Predicted variation of v displacement with z is linear except near the upper boundary

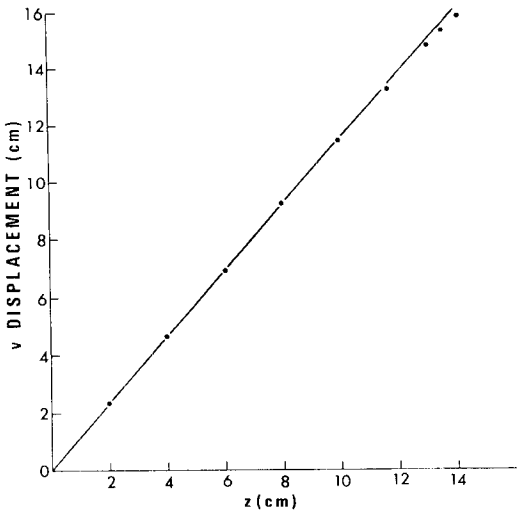

FIG. 8. Variation of tangental displacement with z for model I-3 at $r = 1$.

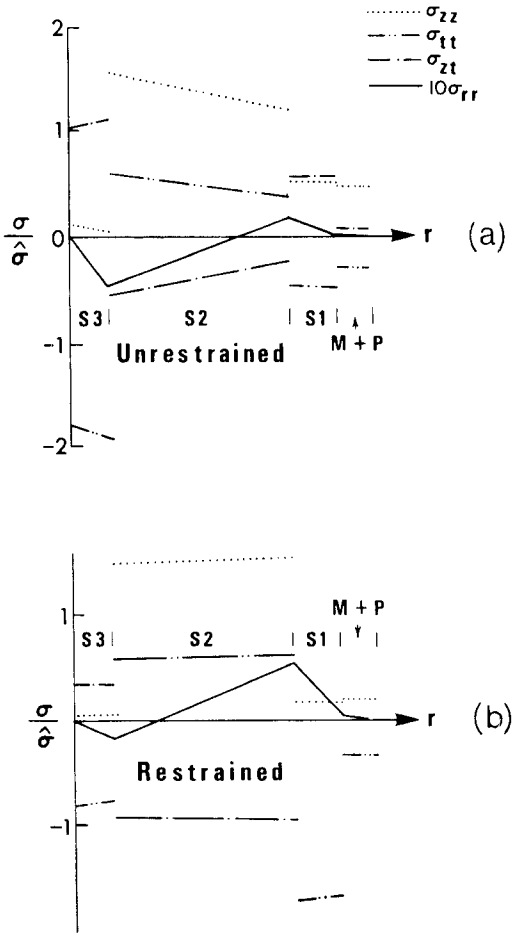

FIG. 9. Stress distribution for model I-3 with no boundary shear restraint (a) and with boundary shear restraint (b) calculated using finite-element model.

of the model where end effects exist. The rate of twisting ϕ per unit length of fiber for unit elongation is predicted for the models studied based on the v displacement at z = 2:

$$\phi = \frac{v_{2.0}}{2r_{max}} \quad . \tag{15}$$

Therefore:

$$\phi = \frac{v_{2.0}}{2} \quad . \tag{16}$$

The radial distribution of stress obtained for model I-3 using finite-element methods is plotted in Fig. 9. Corresponding model

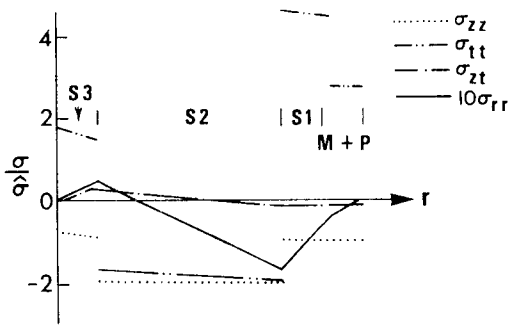

FIG. 10. Stress distributions obtained for model I-3 according to Tang (1972).

results obtained by Tang (1972) are given in Fig. 10. Plotted stresses were computed at the center of the first row of elements. The distribution of stresses in models with boundary shear restraint was also studied using finite-element methods, and Fig. 9b shows the stress distribution for model I-3 when v displacements on the boundary r = 1 are specified equal to zero (i.e. boundary shear restraint). The v displacement at z = 2 and relative angles of twist are given in Table 1 with corresponding results of Tang (1972) for all six models.

An estimate of the angle of twist of a cylinder cell can be obtained on the basis of the composite stiffness of the wall material (Schniewind and Barrett 1969). For two-dimensional analyses, the composite wall compliances are given by

$$[\hat{S}] = [P_j (C)_j]^{-1} \tag{17}$$

where P_j = volume proportion of the j^{th} layer. Application of a normal axial stress will produce, in general, shear and normal strains according to

$$\begin{Bmatrix} \varepsilon_{tt} \\ \varepsilon_{zz} \\ \gamma_{zt} \end{Bmatrix} = \begin{Bmatrix} \hat{S}_{12} \\ \hat{S}_{22} \\ \hat{S}_{32} \end{Bmatrix} \sigma_{zz} \tag{18}$$

The angle of twist for a corresponding thin-walled cylinder of unit length and radius would be

$$\phi' = \gamma_{zt} = \hat{S}_{32}\, \sigma_z \quad . \tag{19}$$

TABLE 1.

Model	$v_{2.0}$† (cm)	$\phi = \frac{90}{\pi} v_{2.0}$ (degrees cm^{-1})††	Tang (1972) (degrees cm^{-1})	ϕ'††† (degrees cm^{-1})	ϕ/ϕ'
I-1	1.6108	46.14	110.90	39.71	1.162
I-2	2.3906	68.48	103.02	56.62	1.209
I-3	2.2861	65.49	334.78	57.56	1.138
II-1	3.8545	110.42	193.17	97.60	1.131
II-2	4.7661	136.53	41.79	113.80	1.200
II-3	4.0448	115.87	89.14	104.68	1.108

† transverse displacement at z = 2 cm and r = 1 cm for unit axial strain

†† angle of twist predicted using two-dimensional analysis

††† degrees of twist per unit length of cell of unit external radius under unit axial strain

The angle of twist predicted using two-dimensional analyses is also given in Table 1.

The axial force required to produce unit elongation for restrained and unrestrained models can be estimated from the 2-D analysis. For a unit area the axial force is given by $P = 1/S_{22} \cdot 1$ for unrestrained cells and for restrained cells

$$P = 1/\left(S_{22} - \frac{S_{23}^2}{S_{33}}\right) . \qquad (20)$$

Predicted axial forces are shown in Table 2 in comparison to results obtained from the finite-element analysis.

DISCUSSION OF RESULTS

The results of the finite-element stress analysis shown in Figs. 9a and 9b are internally consistent in that the relative tangential stresses integrate to 0.00 ± 0.02 over the radius of the cell and the relative axial stresses integrate to 1.00 ± 0.02 for all models studied. The results (Fig. 9a) differ substantially from the results obtained by Tang. Since Tang's approach is questionable and his results were obviously inconsistent as already discussed, little would be gained by detailed comparisons.

It would be of interest, however, to make a comparison between results obtained by two-dimensional and three-dimensional analyses. Results for single model fibers with identical structural details and material parameters are not available from the literature, since as previously stated the results of Mark and Gillis (1970) cannot be used for this purpose. Such a comparison can be made on the basis of the calculated values of relative angle of twist shown in Table 1 and axial forces shown in Table 2. As may be expected on the basis of the divergence in results for stress distribution, there is little numerical resemblance between the data of Tang and those obtained by the finite-element method. There is, however, fairly good agreement between finite-element results and those of the two-dimensional analysis, as may be seen from Tables 1 and 2. Twisting angles predicted by finite-element methods are from 11 to 20% larger than estimated by two-dimensional methods, but maximum axial forces differ by less than 3%. Similar strain fields imply similar stress fields, and

TABLE 2.

Model	Unrestrained		Restrained	
	Finite Element	2-D	Finite Element	2-D
I-1	0.4965 x 10^{11}dynes	0.5028 x 10^{11}dynes	0.7631 x 10^{11}dynes	0.7754 x 10^{11}dynes
I-2	1.0640	1.0826	3.3756	3.4571
I-3	0.7507	0.7531	1.7395	1.7607
II-1	0.6486	0.6495	1.6892	1.7013
II-2	1.6280	1.6316	8.6656	8.7886
II-3	1.4683	1.4366	3.9580	3.9758

hence our results do not indicate major differences in the nature of the stress distributions predicted by two- and three-dimensional analyses. A significant exception is that the two-dimensional analysis is incapable of predicting radial stresses. Since radial stresses are always less than 10% of the axial mean stress (Figs. 9a and b), this may not be a serious detriment for 2-D analysis thin-walled models of wood fibers. Comparing parts a and b of Fig. 9 shows that introduction of shear restraint tends to reduce the radial variation of stress and the maximum values of the normal stresses, particularly in the S2 layer. This indicates that an improved mechanical efficiency may be obtained when the fiber is restrained. Obviously, this is not totally unexpected since the fiber actually does have boundary restraint in its natural environment. Shear stresses predicted for the S1 and M + P layers in the unrestrained models vanish on the application of boundary shear restraint, verifying the assertion presented earlier.

No attempt was made to allow for variations in microfibril angles in the radial as compared to the tangential walls of a given cell. Some type of law of mixtures approach might be used to calculate angle of twist, but of course this would not lead to a suitable assessment of stresses in such a double-composite model. The data used by Tang indicate that three-fourths of the wall area is radial wall and one-fourth tangential wall—in other words a highly flattened cell cross section. A cylindrical model may not be very appropriate for such a cell shape. A real cell of more nearly circular cross section, on the other hand, would probably not have a very large difference in microfibril angles in the two wall areas. For a highly flattened cell cross section, a different finite-element formulation that allows for a more realistic geometric modelling would be preferable.

The close agreement between finite-element results and the two-dimensional predictions for the models studied has shown the value of the two-dimensional analysis techniques for the analysis of thin-walled cells that can be considered to have a circular cross section. The finite-element method presented, however, represents a powerful approach of great general validity, which will also allow accurate assessment of stresses in thick-walled, circular, cylinder models.

REFERENCES

GILLIS, P. P., AND R. E. MARK. 1973. Analysis of shrinkage, swelling, and twisting of pulp fibers. Cellul. Chem. Technol. 7:209–234.

LEKHNITSKII, S. G. 1963. Theory of elasticity of an anisotropic elastic body. Holden-Day Inc., San Francisco, Calif.

MARK, R. E., AND P. P. GILLIS. 1970. New models in cell-wall mechanics. Wood Fiber 2(2):79–95.

SCHNIEWIND, A. P. 1972. Elastic behavior of the wood fiber. *In*: B. A. Jayne, ed. Theory and design of wood and fiber composite materials. Syracuse Univ. Press, Syracuse, N.Y.

SCHNIEWIND, A. P., AND J. D. BARRETT. 1969. Cell-wall model with complete shear restraint. Wood Fiber 1(3):205–214.

TIMOSHENKO, S., AND J. N. GOODIER. 1951. Theory of elasticity. McGraw-Hill, New York.

TANG, R. C. 1972. Three-dimensional analysis of elastic behavior of wood fiber. Wood Fiber 3(4):210–219.

ZIENKIEWICZ, O. C. 1971. The finite element method in engineering science. McGraw-Hill, London.